Thermal fluctuations in superconductor/ferromagnet nanostripes

U. Nasti,[1] L. Parlato,[1,2] M. Ejrnaes,[2] R. Cristiano,[2,*] T. Taino,[3] H. Myoren,[3] Roman Sobolewski,[4,5] and G. Pepe[1,2]

[1]*Dipartimento di Fisica, Università degli Studi di Napoli Federico II, I-80125 Napoli, Italy*

[2]*CNR-SPIN Institute of Superconductors, Innovative Materials and Devices, UOS-Napoli, I-80125 Napoli, Italy*

[3]*Graduate School of Science and Engineering, Saitama University, 338-8570 Saitama, Japan*

[4]*Institute of Electron Technology, PL-02668 Warszawa, Poland*

[5]*Departments of Electrical and Computer Engineering and Physics and Astronomy, and Laboratory for Laser Energetics, University of Rochester, New York 14627-0231, USA*

(Received 25 February 2015; published 6 July 2015)

Thermal fluctuations in hybrid superconductor/ferromagnetic NbN/NiCu bilayers, as well as in pure superconducting NbN, two-dimensional (2D), nanostripes, have been investigated in order to understand the origin of dark counts in superconducting nanostripes when operated as single-photon detectors in the temperature range from 4.2 to 8 K. In 2D superconductors, the dynamics of vortex motion play a significant role in the formation of a transient normal state, leading to dark-count events in current-biased nanostripes. By introducing a weak ferromagnetic overlayer on top of pure NbN, we managed to control the vortex dynamics, which subsequently enabled us to differentiate between several proposed theoretical models. In particular, a 6 - nm - thick NiCu film grown on top of 8 - nm - thick NbN nanostripes led to an enhanced critical current density in the resulting nanostructure, as well as significantly lowered fluctuation rates, as compared to pure NbN structures, leading to reduced dark counts. The enhancement of pinning in NbN/NiCu bilayers provided evidence that thermal excitations of single vortices (vortex hopping) near the edge of a 2D nanostripe were the dominant mechanism of the observed dark-count transients. On the other hand, in pure NbN the leading source of thermal fluctuations was the current-assisted thermal unbinding of vortex-antivortex pairs.

DOI: 10.1103/PhysRevB.92.014501 PACS number(s): 85.25.Pb, 74.78.−w, 75.70.−i, 74.45.+c

I. INTRODUCTION

The problem of fluctuations in two-dimensional (2D) superconducting stripes with a thickness d much smaller than the London penetration depth λ and a width w much smaller than the Pearl length $\Lambda = 2\lambda^2/d \gg w$ has been extensively discussed in the context of the Berezinsky-Kosterlitz-Thouless (BKT) transition [1,2]. The interest in this topic has been revived recently [3,4] to try to better understand the physics of superconducting single-photon detectors (SSPDs) consisting of nanostripes that are densely packed into a meander-type geometry. The first SSPDs introduced in 2001 [5] have since received great attention, because of their excellent performance as ultrafast, highly efficient counters for both infrared and visible light photons, and are now regarded as the devices of choice in such high-performance applications as quantum optics and quantum communications [6,7]. The SSPD operation principle is based on a supercurrent-to-resistive-state transition of a 2D nanostripe maintained at a temperature far below the critical temperature T_C and biased sufficiently close to its critical current I_C. The energy of one or several optical photons absorbed in the nanostripe is sufficient to trigger the transition, producing a transient resistive state and resulting in a detection event.

Independently of the photon counts described above and even when completely isolated from any external light, the SSPD spontaneously generates (especially at higher operating temperatures and with the bias close to I_C) transient voltage pulses, generally known as dark counts. Fully understanding the nature of dark counts, i.e., the physical mechanism of these fluctuation events is very relevant for optimizing the counting performance of SSPDs (minimization of their dark counts). In addition, the dark-count phenomenon has its own basic physics interest in relation to dissipation and thermal fluctuations effects occurring in superconducting 2D nanostripes and 1D (one-dimensional) nanowires.

The present literature on dark counts in SSPDs focuses exclusively on NbN-based devices [3,4,8,9] and most recently favors the explanation that assigns the most relevant role to magnetic vortices moving across the width of a superconducting stripe, either as vortex-antivortex (VAP) pairs or as single vortices overcoming the barrier at opposite edges of the stripe—a mechanism called vortex hopping (VH). In other proposals, relevant mechanisms consider thermal fluctuations of the number of excitations [8], or spontaneous nucleation of normal-state regions across the stripe in analogy with 2π−phase slip centers existing in 1D wires [10,11], but the latter process is typically discarded because its occurrence has a low probability in 2D superconducting nanostripes, typically implemented in practical SSPDs.

Besides NbN, a number of superconducting materials have been most recently proposed and successfully implemented for SSPD applications, for example, WSi and MoSi [12,13] or hybrid superconductor/ferromagnet (S/F) bilayers [14]. Therefore, it is important to note that the composition and morphology of different materials may lead to significant variations in fluctuation mechanisms. In this respect, the investigation of S/F bilayers is of particular interest because, as we have already demonstrated elsewhere [14–16], the presence of a weak ferromagnetic overlayer significantly influences both the superconducting and optical properties of the S/F nanostripes. In fully proximitized, hybrid S/F nanostructures, such as NbN/NiCu (NiCu alloy is a weak ferromagnet),

*Corresponding author: roberto.cristiano@cnr.it

vortex pinning effects are certainly of relevance, leading, e.g., to the J_C enhancement [14]. At the same time, even an epitaxial-quality S/F interface leads to a significant change in the electron nonequilibrium relaxation dynamics observed in photoresponse experiments [15,16]. Consequently, the S/F systems constitute a great test bed for investigating the role of magnetic vortices in fluctuation phenomena in 2D superconducting nanostripes and can provide a direct comparison between various models that have been proposed in literature. The latter is greatly facilitated by the fact that all test structures, as well as the pure-S reference samples, can be processed in the same fabrication run and tested under exactly the same conditions. Finally, besides their unquestionable role in dark counts, vortices have also been implicated as a possible reason for the appearance of photon counts in SSPDs, at least as a supplementary detection mechanism [17,18]. They are, in fact, likely to play a key role in the nonequilibrium photoresponse mechanism of high-temperature superconducting photodetectors [19].

In this work we investigate the effects of thermal fluctuations in superconducting hybrid S/F nanostructures and compare them with those observed in pure-S nanostripes. Our hybrid S/F samples are 5 -μm - long, 100 - nm - wide nanostripes that consist of an 8 - nm - thick NbN film covered with a 6 - nm - thick NiCu, weak ferromagnet overlayer, while the reference samples are 5 -μm - long, 175 - nm - wide, 8 - nm - thick NbN, pure-S nanostripes. The experimental dependences of the fluctuation rates as functions of bias current and temperature are presented and discussed in the framework of both the VAP and VH theoretical models. We also provide arguments for why we excluded other possible fluctuation mechanisms and, instead, focused only on the VAP and VH scenarios. Most importantly, our studies, as suggested by Bartlof *et al.* [3], enabled us to differentiate between the VAP and VH models.

This paper is organized as follows: Sec. II describes our sample fabrication and characterization, as well as presents time-resolved dark- and photon-count waveforms and measurements of the thermal fluctuation rates versus the bias current and temperature. Section III outlines the main features of both the VAP and VH theoretical models, which we then used to interpret our experimental data. Finally, Sec. IV presents our conclusions and future outlook.

II. EXPERIMENTAL DETAILS AND RESULTS

The base of superconducting nanostripes tested in this work was 8 - nm - thick NbN film grown on MgO substrates by reactive dc-magnetron sputtering in an Ar/N_2 gas mixture under the general sputtering conditions reported elsewhere [14–16]. For S/F structures, a NiCu overlayer was deposited in the same system, without breaking vacuum, by a dc magnetron in pure Ar equipped with a $Ni_{0.39}Cu_{0.61}$ target at a 155 - W deposition power and a rate of 60 nm/min, respectively. Magnetic moment tests demonstrated that our NiCu overlayers were ferromagnetic with a Curie temperature of about 20 K. All tested nanostripes were patterned by electron-beam lithography, followed by reactive-ion etching. Gold contacts were defined by conventional photolithography and the lift-off method. For thermal fluctuation measurements,

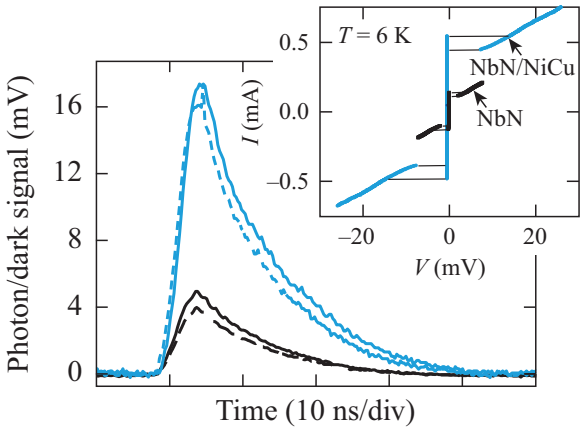

FIG. 1. (Color online) Photon- and dark-count pulses of NbN (black solid and dashed lines, respectively) and NbN/NiCu (light blue solid and dashed lines, respectively) nanostripes. All pulses were recorded under the same conditions, namely, $I_b/I_C = 0.8$ and $T = 4.9$ K. For photon illumination, we used 6.25 - ns - wide laser pulses with a 1550 - nm wavelength. The inset shows typical, hysteretic I-V characteristics collected for both NbN (black solid line) and NbN/NiCu (light blue solid line) nanostripes at 6.5 K.

we used 5 -μm - long straight nanostripes with a width of 100 and 175 nm for NbN/NiCu and NbN, respectively. The NbN stripes exhibited $T_C = 12.1 \pm 0.2$ K, while the T_C values of the NbN/NiCu samples were suppressed by less than 0.5 K.

Our test structures were measured at temperatures ranging from 4.2 to 8.0 K, i.e., much lower than T_C, as required for typical operation of an SSPD and, at the same time, optimized for our fluctuation studies, since lower operating temperatures would result in very sparse dark counts. Correspondingly, current-voltage (I-V) characteristics collected for our nanostripes were always hysteretic (see inset in Fig. 1 as an example) and in all cases we observed that for NbN/NiCu stripes the I_C values (based on a simple 5 - μV criterion) were over 3 times larger than the ones for pure NbN stripes. Subsequently, we confirmed that the obtained temperature dependences of critical-current densities, $J_C^{NbN/NiCu}(T)$ and $J_C^{NbN}(T)$, for NbN/NiCu and NbN nanostripes, respectively, were in good agreement with our previously published experiments [14]; J_C's for NbN/NiCu nanostructures were significantly enhanced, reaching at 4.2 K $J_C^{NbN/NiCu} = 43.2\,MA/cm^2$, while $J_C^{NbN} = 11.6 MA/cm^2$. Following [14], we believe that in fully proximitized S/F film, the magnetic overlayer can be considered as a network of scalar impurities that generate extra flux pinning [20].

To measure the dark-count rate, we mounted our samples on a cryogenic insert and placed them inside a liquid-helium transport Dewar. The sample holder was surrounded by a metallic enclosure that completely shielded the test structure from outside radiation. The sample temperature was controlled by varying the helium vapor pressure and position of the insert inside the Dewar and was measured with a calibrated germanium thermometer. The dark-count events were registered as voltage fluctuation transients and readout using a cascade of two microwave amplifiers with an effective bandwidth of 0.1 to 100 MHz and a total gain of 20 dB. The amplified signals

were fed by a 50 - Ω coaxial cable into our readout electronics, which consisted of either a digital oscilloscope with a 1 - GHz bandwidth or a pulse counter with a 100-MHz bandwidth.

As a reference, we have also measured photon counts by illuminating the same nanostripes with 6.25 - ns - wide, 1550 - nm - wavelength laser pulses, generated by a laser diode with a repetition rate of 80 MHz. The laser-spot diameter was $\sim 50\,\mu$m, much larger than the size of the nanostripe, ensuring a uniform optical illumination. The latter tests were done in a continuous-flow helium cryostat with an optical window.

The main panel in Fig. 1 presents examples of time-resolved waveforms of dark (solid lines) and photon (dashed lines) counts, measured at $T = 4.9$ K for both NbN/NiCu and NbN nanostripes biased at the same value of a normalized bias current, namely $I_b/I_C = 0.8$. We note that for each nanostripe the dark- and photon-count pulses practically overlap since in both cases the transient voltage signals reflect the resistive state of a nanostripe. Actually, all four waveforms in Fig. 1 have the identical shape with a detection-system-limited rise time and an ~ 20 - ns - long fall time. The difference in the amplitude between the NbN/NiCu and NbN signal pairs (the S/F pulses exhibit significantly larger amplitudes) is a result of the earlier-mentioned enhancement of $J_C^{\mathrm{NbN/NiCu}}(T)$; in fact, the pulse amplitude ratio is very close to the $J_C^{\mathrm{NbN/NiCu}}/J_C^{\mathrm{NbN}}$ ratio at 4.9 K.

Figure 2 presents thermal fluctuation or dark-count rates of NbN (black squares) and NbN/NiCu (red circles) nanostripes

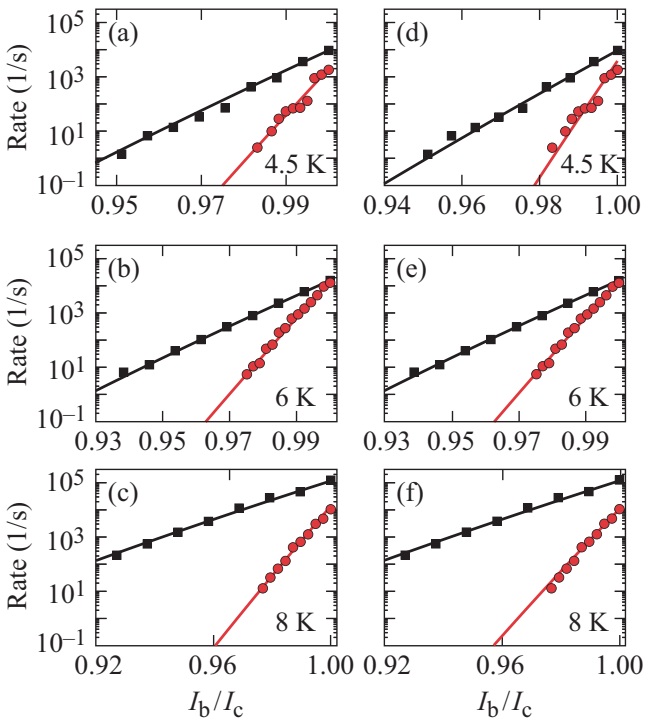

FIG. 2. (Color online) Measured fluctuation rates versus normalized bias current of NbN (black squares) and NbN/NiCu (red circles) nanostripes, measured at 4.5, 6.0, and 8.0 K. The solid lines are the best fits obtained using the (a)–(c) VAP model and the (d)–(f) VH model.

as functions of I_b/I_C at temperatures 4.5, 6.0, and 8.0 K, collected using a pulse counter. For both nanostripes we observed that the fluctuation rates decrease exponentially over four orders of magnitude. The S/F sample is, however, much more stable against fluctuations, exhibiting significantly lower dark counts at each temperature. In all panels in Fig. 2, the I_b/I_C range of our measurements was limited by the 1-Hz accuracy of our counter. Finally, we stress that the experimental data (black squares and red circles) presented in Figs. 2(a)–2(c) are exactly the same as those in Figs. 2(d)–2(f). The difference is that the former data set was fitted (solid lines) using the VAP model, while the latter data set was fitted using the VH model. The details of the fits and their physical significance will be presented in the next section.

III. FLUCTUATION MODELS AND DISCUSSION

All our tested nanostripes can be considered as 2D superconducting systems (see Introduction). Their thickness d is much shorter than λ and comparable to the Ginzburg-Landau coherence length ξ. Literature [3,9] values of $\xi_0 = \xi(T = 0)$ for NbN are of the order of a several nanometers, and from superconducting fluctuation measurements [21], we expect that ξ_0 for NbN/NiCu is in the same, several-nanometer range. At the same time $w \ll \Lambda$; therefore, the J_C distribution can be assumed to be homogeneous across the stripe width. Moreover, w is wide enough to nucleate propagation of vortices, since the Likharev condition, $w \geqslant 4.4\,\xi$, is always satisfied.

Various mechanisms are able to produce dark counts and could be considered as responsible for the fluctuation rates measured in our experiments. We can summarize them as (1) thermal unbinding of VAPs, (2) thermal or quantum mechanism of VH, (3) fluctuations of the number of quasiparticles, and (4) thermal or quantum phase-slip center processes. Following the arguments given in [3], based on a comparison of the amplitudes of the excitation energy barriers, we can conclude that the probability of an occurrence of phase-slip centers is very low, so we can ignore this process. Next, following a theoretical approach presented in [8], we calculated the dark-count rate related to the fluctuation in the number of quasiparticles, but any attempt to fit our data with this model failed, in particular for the S/F sample. Finally, since the temperature interval investigated in this work is 4.2 to 8.0 K, we can also exclude fluctuation mechanisms caused by quantum tunneling of vortices through the edge barrier because they become relevant only at sub-Kelvin temperatures [11].

Based on the above, we limit our discussion to the thermal regime and consider only the VAP and VH fluctuation scenarios:

(1) VAP: unbinding of vortex-antivortex pairs and their movement across the nanostripe to its opposite edges resulting from the Lorentz force.

(2) VH: thermal excitation of a single vortex near the edge of the stripe and a consecutive dissipative movement across it.

In both models, thermal fluctuations must overcome an excitation energy barrier $U(I_b,T)$ and the corresponding fluctuation, or, equivalently, the dark-count rate may be

expressed as

$$\Gamma(I_b,T) = \Omega \exp[-U(I_b,T)/k_B T], \quad (1)$$

where Ω is the attempt frequency. The actual expressions for $U(I_b,T)$, as well as the fit values of Ω, will, of course, be different in these two types of mechanisms.

A. Unbinding of vortex-antivortex pairs

In 2D systems, the collapse of a long-range order gives rise to so-called topological defects in the order parameter that, in thin superconducting films, excite pairs of vortices, according to the BKT model. At temperatures below the BTK transition, these pairs consist of single vortices with their respective supercurrents circulating in opposite directions and result in a bound VAP state. Under the $w \geqslant 4.4\xi$ condition, a BKT phase transition can occur only if the energy of a bound VAP depends logarithmically on the separation distance of the vortex core centers $r (r \ll \Lambda)$. Under a transport current condition, however, a Lorentz force is exerted on VAPs and directed in opposite directions for the vortex and the antivortex, respectively. The resulting torque forces VAPs to align perpendicularly to the current flow. The binding energy changes with the angle and reaches its minimum at $\pi/2$. As it was shown by Mooji [22], the interplay between repulsion of vortices in a pair due to the Lorentz force and their magnetic attraction defines the current-dependent $r = 2.6\xi I_C/I_b$, leading to the minimal binding energy of the pair U_{VAP} [3].

This binding energy may be overcome by thermal excitations with a probability equal to the Boltzmann's factor $\exp[-U_{\mathrm{VAP}}/k_B T]$. In the absence of pinning, thermally unbound vortices will move freely toward opposite edges of the strip, where they leave the structure or rather annihilate with an oppositely orientated vortex. The moving vortices dissipate energy, initiating creation of a nonsuperconducting domain. In current-biased ($I_b < I_C$) stripes, appearance of such domains results in voltage transients that are then registered as dark-count events. According to the model in [3] and [8], the dark-count rate follows Eq. (1) with the U_{VAP} given by

$$U_{\mathrm{VAP}} = \frac{A(T)}{\varepsilon}\left[\ln\left(\frac{2.6 I_C}{I_b}\right) - 1 + \frac{I_b}{2.6 I_C(T)}\right], \quad (2)$$

where $A(T)$ is the vortex interaction constant and ε is the averaged polarizability of a VAP within the entire VAP population [3,22].

The solid lines in Figs. 2(a)–2(c) present the fits of the fluctuation rates for both NbN and NbN/NiCu samples based on Eqs. (1) and (2) at three different temperatures. The values of the fitting parameters $A(T)$ and ε are reported in Table I [23]. We note that the fits are in the excellent agreement with the experimental data and the $A(T)$ and ε values are reasonably close to that reported in literature [3]. Interestingly, the A parameter for the NbN/NiCu sample has a value about three times greater than that for the NbN sample, indicating that the binding energy of the VAP in the S/F bilayer is significantly stronger than that in a pure NbN. The latter explains the dramatically lower (over an order of magnitude) fluctuation rates for the NbN/NiCu nanostripe, as compared to NbN. In addition, an increase of ε provides clear evidence that a weak ferromagnetic NiCu top layer leads to enhanced pinning in the S/F sample.

B. Vortices overcoming the edge barrier

We have also analyzed our experimental data in a framework of the motion of single unbounded vortices [3,4]. At bias currents close to the depairing I_C, the magnetic self-field at the stripe edges is much larger than the critical field for vortex entry. The entry of vortices at one edge of the stripe and antivortices at the opposite edge is prohibited by an edge barrier very similar to the Bean-Livingston surface barrier [3,24]. Consequently, the corresponding probability for thermally activated vortex hopping over this energy barrier is again proportional to the Boltzmann factor $\exp[-U_{\mathrm{VH}}/k_B T]$. However, U_{VH} is now given by

$$U_{\mathrm{VH}}(T,I_b) = E_B(T,I_b)\left(\ln\left\{\frac{2w}{\pi\xi(T)}\frac{1}{\sqrt{1+\left[\frac{\Phi_0 I_b}{\pi E_B(T,I_b)}\right]}}\right\} - \frac{\Phi_0 I_b}{\pi E_B(T,I_b)}\left\{\arctan\left[\frac{\pi E_B(T,I_b)}{\Phi_0 I_b}\right] - \frac{\pi\xi(T)}{2w}\right\}\right), \quad (3)$$

where $E_B(I_b,T) = \Phi_0^2/2\pi\mu_0\Lambda(I_b,T)$ is the energy scale [3].

Once a vortex jumps over the barrier, thanks to the Lorentz force, it will move across the stripe. Analogically to the VAP scenario, motion of these free vortices creates a nonsuperconducting domain in the stripe and results in a voltage transient. The resulting dark-count rate for the VH process is given by Eq. (1) with U_{VH} defined in Eq. (3).

In Figs. 2(d)–2(f) the solid lines are the fits of the experimental fluctuation rates (circles) for the NbN and NbN/NiCu samples, but this time using Eqs. (1) and (3), i.e., the VH model. We note that these fits (except of the NbN/NiCu data at 4.5 K, where the fit is not perfect) are as excellent as in the case of the VAP model. The E_B and ξ fitting parameters are reported in Table I [23] next to the column representing the VAP model. First of all, we notice a clear self-consistency of our thermal fluctuation approach, i.e., that we indeed have $E_B = A/2$, as expected from the definition of E_B. The extracted value of E_B allowed us to calculate the parameter Λ and, consequently, λ for our samples at the three temperatures studied. The actual values are listed in a separate column in Table I, and we note that for NbN/NiCu, both Λ and λ are quite substantially reduced as compared to NbN, again, stressing their enhanced 2D character.

The $\xi(T)$ values obtained with the fitting procedure of the VH model for both NbN and NbN/NiCu nanostripes (see Table I) are plotted in Figs. 3(a) and 3(b), respectively, as a function of normalized temperature T/T_C. As expected earlier, the presence of the NiCu overlayer enhances the S/F nanostripe 2D character by reducing the $\xi(T)$ values, as compared to the pure NbN sample. The solid lines are the best

TABLE I. Parameters used to fit the measured fluctuation rates within the VAP and VH models.

		VAP model fitting parameters		VH model fitting parameters		Calculated parameters	
Samples	$T(K)$	A(eV)	ε	ξ(nm)	E_B(eV)	$\Lambda(\mu$m)	λ(nm)
NbN	4.5	0.20	1.9	4.5	0.10	34	368
	6.0	0.19	1.8	5.9	0.09	37	385
	8.0	0.16	1.8	6.9	0.08	44	420
NbN/NiCu	4.5	0.70	3.0	4.1	0.34	9.7	261
	6.0	0.66	2.5	5.0	0.34	10.3	269
	8.0	0.65	2.0	6.0	0.33	10.4	270

fits of these values obtained by using the following analytical expression [Eq. (3)]:

$$\xi^2(T/T_C) = \frac{\xi_0^2}{(1-T/T_C)}\frac{1}{\sqrt{1+T/T_C}}. \quad (4)$$

Although the $\xi(T)$ values extracted from the fits carry rather large errors (especially at higher temperatures), the agreement with Eq. (4) is still very good and allows us to estimate the ξ_0 values as equal to 3.9 and 4.2 nm for the NbN/NiCu and NbN samples, respectively. A slightly reduced ξ_0 value for the S/F bilayer reinforces the enhanced D character of these nanostructures.

C. Discussion

A simple "visual" comparison between the fits representing the VAP and VH models and presented in Figs. 2(a)–2(c) and 2(d)–2(f), respectively, does not enable us to differentiate which of the two vortex-based scenarios best describes the physics of our experiments. Clearly we deal with thermal excitations and their probability in both cases is equal to the Boltzmann's factor, resulting in a single exponential fit. The possible difference should be related to the different values of the excitation energy barrier $U_{\rm VAP}$ and $U_{\rm VH}$, defined by Eqs. (2) and (3), respectively. Therefore, we have attempted a more quantitative approach by plotting the values of $U_{\rm VAP}$ and $U_{\rm VH}$ in units of $k_{\rm B}$ at the fixed $I_b/I_C = 0.99$ bias as functions of temperature. The results are plotted in Fig. 4. The points correspond to the excitation energy barrier values $U_{\rm VAP}/k_{\rm B}$ and $U_{\rm VH}/k_{\rm B}$, representing the best fits obtained from Fig. 2, for both the NbN and NbN/NiCu samples (see Fig. 4 caption for details), and the solid lines are only guides for the eye.

Now we can make individual comparisons between the data corresponding to S/F and S samples within the same fluctuation model, as well as compare the VAP and VH models for the same sample type. Within the VAP model, the data for NbN (red circles) show that the excitation energy of the pure NbN sample is always significantly smaller than that of the NbN/NiCu (magenta inverted triangles) sample, i.e., $U_{\rm VAP}^{\rm S} < U_{\rm VAP}^{\rm S/F}$. The same behavior (although not as dramatic) is also observed within the VH model. Again, for NbN (black squares) vs NbN/NiCu (blue triangles) data, $U_{\rm VH}^{\rm S} < U_{\rm VH}^{\rm S/F}$. The latter is a clear confirmation that, in general, the S/F nanobilayer is characterized by a significantly higher energy excitation barrier, what must correspond to the stronger pinning and, consequently, lead to a significant decrease in the rate of thermal fluctuations (dark counts), as observed in Fig. 2 for the NbN/NiCu nanostripes.

Comparing the two models for the same sample type, i.e., NbN/NiCu (blue triangles) with NbN/NiCu (magenta inverted triangles), and NbN (black squares) with NbN (red circles), we note in Fig. 4 that for the S/F sample, the excitation energy corresponding to the VH model (blue triangles) are always markedly lower than those of the VAP

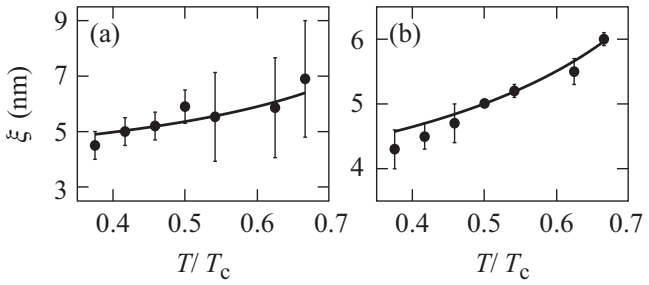

FIG. 3. Coherence length dependence on the normalized temperature for (a) NbN and (b) NbN/NiCu samples. The $\xi(T)$ values (circles) were obtained by the best-fitting procedure [Eqs. (1) and (3)] to the VH model (see also Fig. 2). The solid lines are the best fits obtained by using Eq. (4). The extrapolated values of ξ_0 are 4.2 and 3.9 nm for NbN and NbN/NiCu samples, respectively.

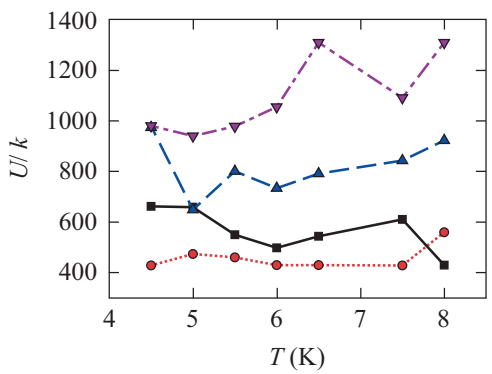

FIG. 4. (Color online) Excitation energy barrier U in units of $k_{\rm B}$ at seven temperatures. The plotted points are the best-fit values from Fig. 2 at $I_b/I_C = 0.99$; the corresponding symbols are magenta inverted triangles: VAP, NbN/NiCu; blue triangles: VH, NbN/NiCu; red circles: VAP, NbN; and black squares: VH, NbN. The lines are only guides for the eye.

model (magenta inverted triangles), i.e., $U_{VH}^{S/F} < U_{VAP}^{S/F}$. Thus, the VH fluctuation mechanism is more probable to occur in the bilayer samples, since it corresponds to the lower value of U. The only exception is the $T = 4.5$ K data point, but as we have already mentioned, the VH fit in this case is not the best [see Fig. 2(d)]. On the other hand, for the pure-S samples, the U_{VAP} and U_{VH} values although quite close, generally exhibit the opposite behavior, i.e., $U_{VAP}^{S} < U_{VH}^{S}$, so the VAP mechanism seems to be preferable. Consequently, based on our experimental results, we conclude that the VH scenario is clearly favored for S/F samples, while the VAP mechanism is more probable for pure NbN samples, supporting earlier findings [9].

IV. CONCLUSIONS

We have measured the fluctuation rate as a function of the applied bias current at various temperatures in hybrid S/F and pure-S nanostripes and have performed the same NbN/NiCu and NbN sample measurements of the I-V characteristics and the time-resolved waveforms of both photon- and dark-count events. The NbN/NiCu samples exhibited an enhancement of J_C; correspondingly, we measured the amplitude increase of both the photon- and dark-count pulses. The latter findings clearly indicate the role of pinning of magnetic vortices in S/F nanostructures and confirm the results obtained previously on similar samples [14]. The measured fluctuation rates have been analyzed in a framework of the VAP and VH theoretical models that are based on thermal activation and subsequent motion of magnetic vortices. In the fluctuation rate versus temperature experiments, we observed that the NbN/NiCu samples were significantly more stable against thermal fluctuation as compared to NbN, and for NbN/NiCu a mechanism, based on thermal VH was clearly dominant. The model discrimination was less evident in the case of pure-S samples; nevertheless, our results points to VAP as the mechanism responsible for the dark counts observed in NbN nanostripes, in agreement with earlier studies [9].

For the practical application of nanostripes as SSPDs, the detailed knowledge of the physical origin of thermal fluctuations is important to improving the performance of superconducting detectors by controlling their dark counts. Hybridization of a pure superconducting nanostripe with a weak ferromagnetic material, as in the case of the NbN/NiCu sample, is very promising since it leads to a significant decrease in thermal fluctuations that corresponds to reduced dark counts, as well as in the increase in the photoresponse amplitude, resulting in an improved signal-to-noise ratio of the SSPD.

ACKNOWLEDGMENT

The authors acknowledge the European Union COST Action MP1201.

[1] Y. Liu, D. B. Haviland, L. I. Glazman, and A. M. Goldman, Phys. Rev. Lett. **68**, 2224 (1992).
[2] J. M. Repaci, C. Kwon, Q. Li, X. Jiang, T. Venkatessan, R. E. Glover III, C. J. Lob, and R. S. Newrock, Phys. Rev. B **54**, R9674 (1996).
[3] H. Bartolf, A. Engel, A. Schilling, K. Il'in, M. Siegel, H. W. Hübers, and A. Semenov, Phys. Rev. B **81**, 024502 (2010).
[4] L. N. Bulaevskii, M. J. Graf, C. D. Batista, and V. G. Kogan, Phys. Rev. B **83**, 144526 (2011).
[5] G. N. Gol'tsman, O. Okunev, G. Chulkova, A. Lipatov, A. Semenov, K. Smirnov, B. Voronov, A. Dzardanov, C. Williams, and R. Sobolewski, Appl. Phys. Lett. **79**, 705 (2001).
[6] R. H. Hadfield, Nat. Photon. **3**, 696 (2009), and references therein.
[7] C. M. Natarajan, M. G. Tanner, and R. H. Hadfield, Supercond. Sci. Technol. **25**, 063001 (2012), Topical Review and references therein.
[8] A. Engel, A. D. Semenov, H.-W. Hübers, K. Il'in, and M. Siegel, Physica C **444**, 12 (2006).
[9] J. Kitaygorsky *et al.*, IEEE Trans. Appl. Supercond. **17**, 275 (2007).
[10] J. S. Langer and V. Ambegaokar, Phys. Rev. **164**, 498 (1967).
[11] D. S. Golubev and A. D. Zaikin, Phys. Rev. B **64**, 014504 (2001).
[12] F. Marsili *et al.*, Nat. Photon. **7**, 210 (2013).
[13] Y. P. Korneeva *et al.*, Supercond. Sci. Technol. **27**, 095012 (2014).
[14] N. Marrocco *et al.*, Appl. Phys. Lett. **97**, 092504 (2010).
[15] D. Pan, G. P. Pepe, V. Pagliarulo, C. De Lisio, L. Parlato, M. Khafizov, I. Komissarov, and R. Sobolewski, Phys. Rev. B **78**, 174503 (2008).
[16] T. Taneda, G. P. Pepe, L. Parlato, A. A. Golubov, and R. Sobolewski, Phys. Rev. B **75**, 174507 (2007).
[17] J. J. Renema, G. Frucci, Z. Zhou, F. Mattioli, A. Gaggero, R. Leoni, M. J. A. de Dood, A. Fiore, and M. P. van Exter, Phys. Rev. B **87**, 174526 (2013).
[18] J. J. Renema *et al.*, Phys. Rev. Lett. **112**, 117604 (2014).
[19] R. Arpaia, M. Ejrnaes, L. Parlato, F. Tafuri, R. Cristiano, D. Golubev, R. Sobolewski, T. Bauch, F. Lombardi, and G. P. Pepe, Physica C **509**, 16 (2015).
[20] A. I. Buzdin, Rev. Mod. Phys. **77**, 935 (2005).
[21] W. Lang (private communication).
[22] J. E. Mooij, in *Percolation, Localization, and Superconductivity*, edited byA. M. Goldman and S. A. Wolf, NATO ASI, Series B, Vol. 109 (Plenum, New York, 1984), p. 325.
[23] The attempt frequency Ω is the third fitting parameter in both models. Our fitted values are close to that of Ref. [3]. They are not shown in Table I because of their irrelevance to the discussion.
[24] C. P. Bean and J. D. Livingston, Phys. Rev. Lett. **12**, 14 (1964).